

Article

2-Arylpropionic Acid Pyrazolamides as Cannabinoid CB₂ Receptor Inverse Agonists Endowed with Anti-Inflammatory Properties

Daniela R. de Oliveira^{1,2}, Rodolfo C. Maia¹, Patrícia R. de Carvalho França^{2,3}, Patrícia D. Fernandes^{2,3}, Gisele Barbosa^{1,2}, Lídia M. Lima^{1,2} and Carlos A. Manssour Fraga^{1,2,*}

- ¹ Laboratório de Avaliação e Síntese de Substâncias Bioativas, Instituto de Ciências Biomédicas, Universidade Federal do Rio de Janeiro, Rio de Janeiro 21920-190, RJ, Brazil
- ² Programa de Pós-Graduação em Farmacologia e Química Medicinal, Universidade Federal do Rio de Janeiro, Rio de Janeiro 21920-190, RJ, Brazil
- ³ Laboratório de Farmacologia da Dor e da Inflamação, Instituto de Ciências Biomédicas, Universidade Federal do Rio de Janeiro, Rio de Janeiro 21941-902, RJ, Brazil
- * Correspondence: cmfraga@ccsdecania.ufrj.br

Abstract: Among the most recent proposals regarding the mechanism of action of dipyrrone, the modulation of cannabinoid receptors CB₁ and CB₂ appears to be a promising hypothesis. In this context, the present work describes a series of five novel pyrazolamides (7–11) designed as molecular hybrids of dipyrrone metabolites and NSAIDs, such as ibuprofen and flurbiprofen. Target compounds were obtained in good overall yields (50–80%) by classical amide coupling between 4-aminoantipyrine and arylacetic or arylpropionic acids, followed in some cases by *N*-methylation of the amide group. The compounds presented good physicochemical properties in addition to stability to chemical (pH 2 and 7.4) and enzymatic (plasma esterases) hydrolysis and showed medium to high gastrointestinal and BBB permeabilities in the PAMPA assay. When subjected to functional testing on CB₁- or CB₂-transfected cells, compounds demonstrated an inverse agonist profile on CB₂ receptors and the further characterization of compound LASSBio-2265 (11) revealed moderate binding affinity to CB₂ receptor ($K_i = 16 \mu\text{M}$) with an $\text{EC}_{50} = 0.36 \mu\text{M}$ ($E_{\text{max}} = 63\%$). LASSBio-2265 (11) (at 1, 3, and 10 mg/kg p.o.) was investigated in the formalin test in mice and a remarkable analgesic activity in the late inflammatory phase was observed, suggesting it could be promising for the treatment of pain syndromes associated with chronic inflammatory diseases.

Keywords: dipyrrone; metamizole; cannabinoid receptors; CB₂ inverse agonists; pyrazolamides; molecular hybridization; NSAID



Citation: de Oliveira, D.R.; Maia, R.C.; de Carvalho França, P.R.; Fernandes, P.D.; Barbosa, G.; Lima, L.M.; Fraga, C.A.M. 2-Arylpropionic Acid Pyrazolamides as Cannabinoid CB₂ Receptor Inverse Agonists Endowed with Anti-Inflammatory Properties. *Pharmaceuticals* **2022**, *15*, 1519. <https://doi.org/10.3390/ph15121519>

Academic Editors: Andrea Duranti and Mary J. Meegan

Received: 2 October 2022

Accepted: 2 December 2022

Published: 6 December 2022

Publisher's Note: MDPI stays neutral with regard to jurisdictional claims in published maps and institutional affiliations.



Copyright: © 2022 by the authors. Licensee MDPI, Basel, Switzerland. This article is an open access article distributed under the terms and conditions of the Creative Commons Attribution (CC BY) license (<https://creativecommons.org/licenses/by/4.0/>).

1. Introduction

The modulation of the endocannabinoid system has received great focus among therapeutic possibilities for treating pain processes [1]. *In vivo* studies have demonstrated the influence of cannabinoid receptors in mediating nociception [2–10]. However, the promotion of central effects attributed to CB₁ receptor activation, such as hypoactivity, hypothermia, and catalepsy [11,12] which can translate into psychoactivity in humans remains of concern. The use of selective CB₂ agonists has emerged as alternative, as these compounds attenuate neuropathic pain without the characteristic side effects of CB₁ activation [13].

The importance of CB₂ receptors in the modulation of nociception is related to their expression in cells of both the immune and the peripheral nervous system and the relationship of endocannabinoids with decreased inflammation has been demonstrated in several inflammatory pain models [14–17]. Activation of the endocannabinoid system has also been associated with decreased leukocyte recruitment and increased production of anti-inflammatory cytokines [18].

Dipyrone (1) is an analgesic and antipyretic drug with spasmolytic action and is widely used in Brazil, Latin America, Germany, Spain, and some African countries [19]. *In vivo* studies suggest its analgesic effect depends on the activation of cannabinoid receptors [20–22], as selective CB₁ antagonists but not CB₂ antagonists [23] block the dipyrone-associated anti-hyperalgesia. It is suggested that activation of cannabinoid receptors results from the action of arachidonic acid (4)-conjugated dipyrone metabolites, as also proposed for paracetamol [20]. Two major pyrazolamine metabolites are detected after administration of dipyrone to humans: 4-methylaminoantipyrine (2), formed after chemical hydrolysis, and 4-aminoantipyrine (3), as product of cytochrome P450 (CYP3A4) enzymatic *N*-demethylation (Figure 1) [21]. The biosynthesis of arachidonylpyrazolamide metabolites could result from the action of fatty acid amide hydrolase (FAAH) [22] and these metabolites, henceforward termed (5) and (6), have demonstrated micromolar affinity for CB₁ and CB₂ receptors, although their intrinsic efficacy profiles have not yet been characterized [20].

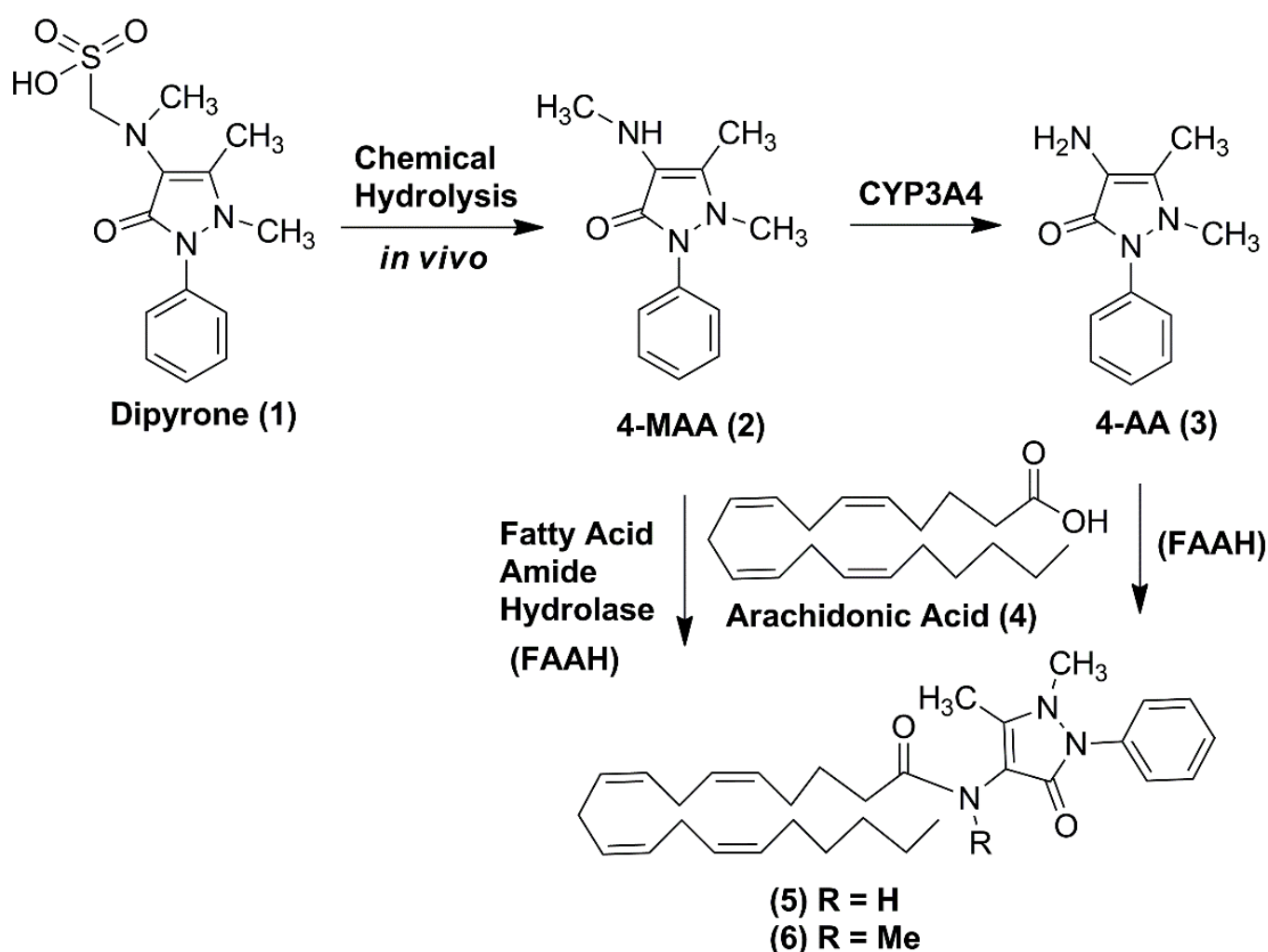


Figure 1. Dipyrone (1) and its active metabolites 4-methylaminoantipyrine (4-MAA, 2) and 4-aminoantipyrine (4-AA, 3) with their corresponding arachidonyl-pyrazolamides (5) and (6), respectively.

The present work describes new structural analogs of arachidonylpyrazolamides, (5) and (6), which exploit the replacement of the arachidonate subunit (A, Figure 2) for a substituted arylacetic or arylpropionic subunit present in some nonsteroidal anti-inflammatory drugs (NSAIDs), especially those belonging to the profen class, due to their well-known relationship with the metabolism of endocannabinoids [24,25].

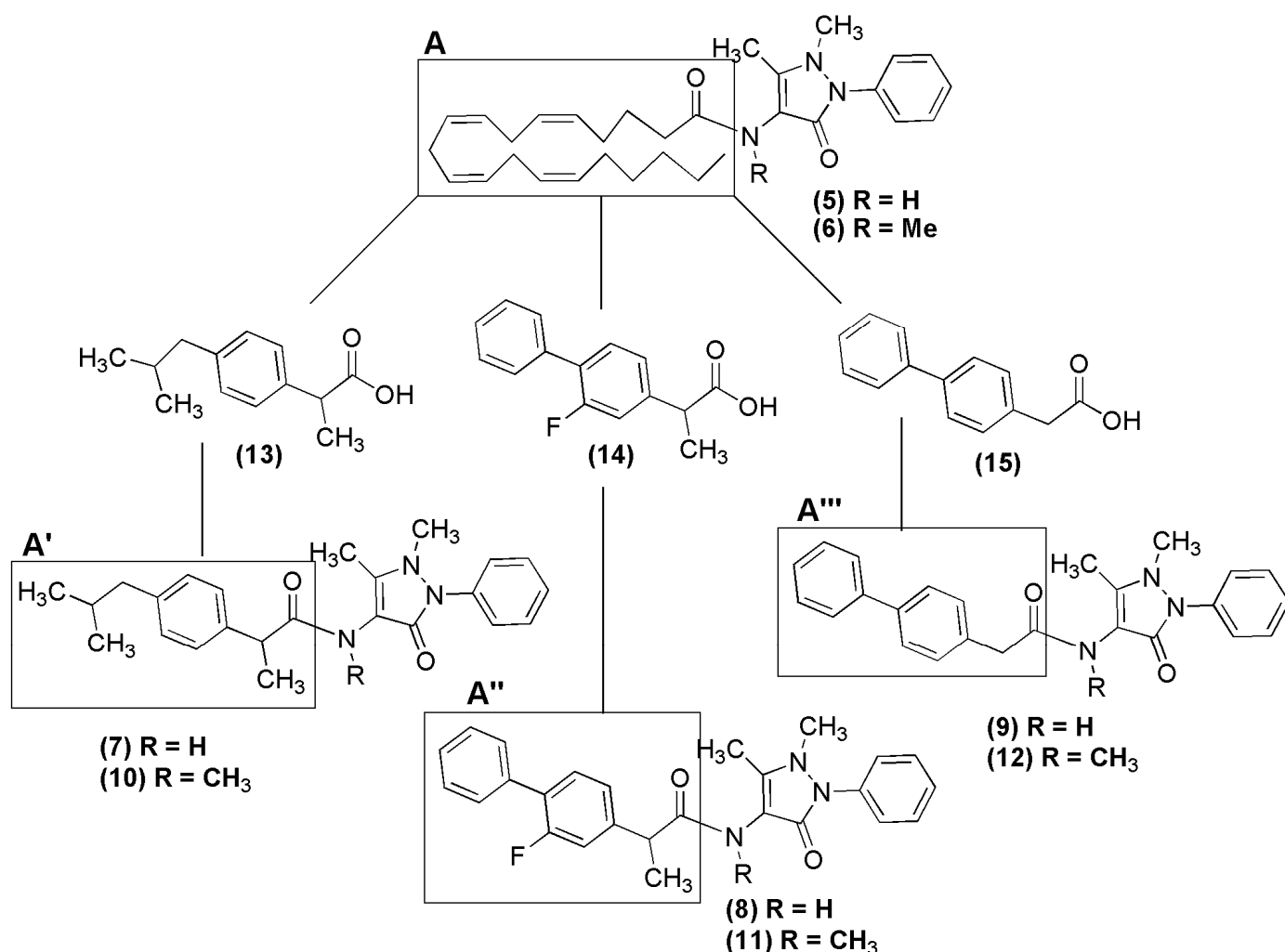


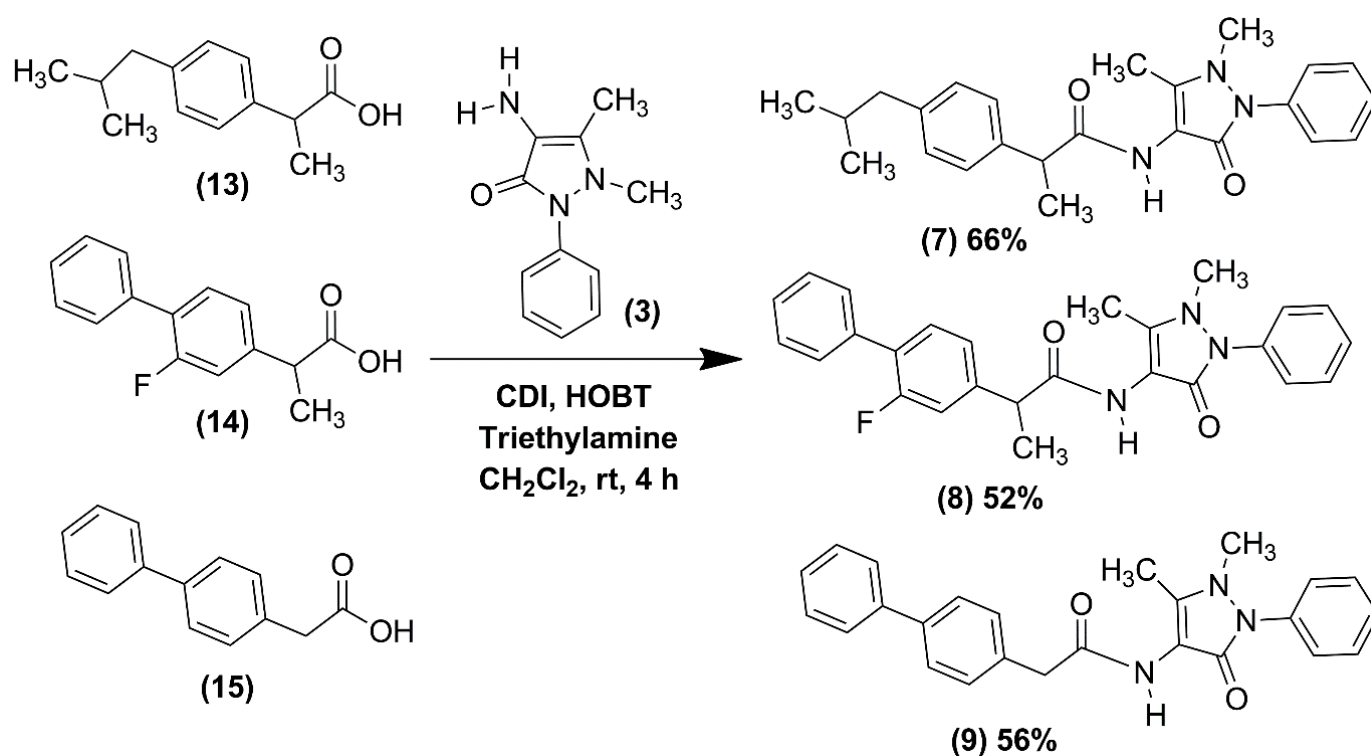
Figure 2. Design concept of novel NSAID-pyrazolamide derivatives (7–12).

The use of arylacetic and arylpropionic NSAIDs in the design of the new compounds (7–12) aimed to mimic the hydrophobic interactions of the alkenyl subunit of arachidonic acid (4) with CB₁ and CB₂, as previously identified in cyclo-oxygenase (COX) enzymes [26]. Therefore, ibuprofen (13) and flurbiprofen (14) were selected as representative NSAIDs for the arylpropionic (profen) class and felbinac (15), an arylacetic derivative structurally related to (14), in order to investigate the influence of the methyl group in the benzylic position. Once synthesized, the target compounds were evaluated regarding their *in vitro* pharmacokinetic profiles and then characterized for their *in vitro* intrinsic efficacy. Moreover, the best compound was submitted to a classical *in vivo* model to confirm its potential as an analgesic drug candidate that acts as a modulator of cannabinoid receptors for the treatment of acute and chronic pain states.

2. Results and Discussion

2.1. Chemical Synthesis of NSAID-Pyrazolamides (7–12)

The target unsubstituted pyrazolamide derivatives (7–9) were synthesized through the classical coupling of a carboxylic acid group of the NSAIDs (13–15) with 4-aminoantipyrine (3) using *N,N'*-carbonyldiimidazole (CDI) and 1-hydroxybenzotriazole (HOBT) as coupling reagents in the presence of triethylamine [27], as illustrated in Scheme 1. The desired pyrazolamides (7–9) were obtained in yields ranging 52–66%.

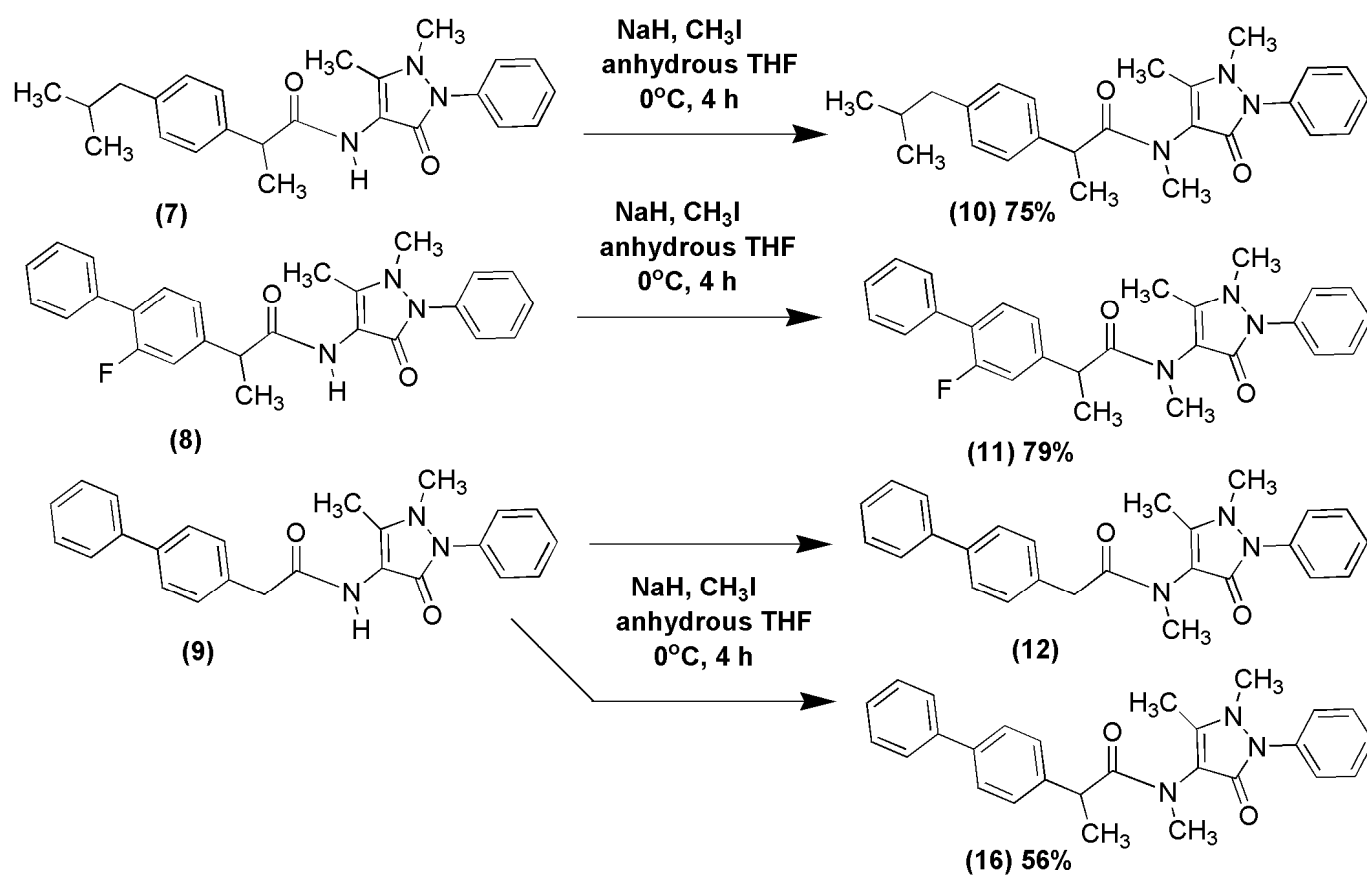


Scheme 1. Synthesis of unsubstituted NSAID-pyrazolamide derivatives (7–9).

Next, pyrazolamides (7–9) were submitted to an *N*-methylation step after treatment with sodium hydride in THF [28], followed by the addition of methyl iodide, as illustrated in Scheme 2. By using these conditions, pyrazolamides **10** and **11** derived from ibuprofen and flurbiprofen, respectively, were prepared in 75% and 79% yields. On the other hand, the expected *N*-methyl carboxamide (**12**) derived from **9** could not be obtained using this methodology, and instead, the bismethylated derivative (**16**) was formed in a 56% yield (Scheme 2). This behavior was associated to the similar pK_a values between the amide and the α -carbonyl hydrogens of **9** [29,30], favoring deprotonation on both sites and bisalkylation to provide compound **16**. Pyrazolamides **7** and **8** were not susceptible to alkylation at the benzylic position due to the steric effect produced by the methyl group originally present.

Attempts to circumvent this problem by changing the base to potassium carbonate in acetone were not successful, and the only product obtained after 48 h was pyrazolamide **16** in low yields. In addition, the use of another strategy that foresaw the initial methylation of Boc-protected **3**, followed by deprotection and coupling with **15**, was also unsuccessful due to the low reactivity of *N*-Boc-pyrazolamide when subjected to alkylation (see Supplementary Material). Therefore, considering that the main motivation for the synthesis of **12** was to evaluate how the absence of the methyl group in the benzylic position could influence the modulation of cannabinoid receptors, we decided to continue the investigation with only the five initially planned pyrazolamides (7–11).

Compounds **7–11** were fully characterized using spectroscopic techniques (see Supplementary Material), and their purity was determined by reverse-phase HPLC analysis and high-resolution mass spectrometry to be greater than 95%, which was considered adequate for the next step of investigating their drug-like properties and biological actions on cannabinoid receptors.



Scheme 2. Synthesis of *N*-methylated NSAID-pyrazolamide derivatives (10–12).

2.2. Drug-like Properties of Pyrazolamides 7–11

After full characterization of compounds 7–11, we proceeded to determine their physicochemical and *in vitro* pharmacokinetic properties, given their strategic relevance for developing novel orally available drug candidates.

Aqueous solubility of pyrazolamides 7–11 was determined at pH 7.4 in phosphate buffer, yielding values within 10–100 μM (Table 1) [31]. These values are considered a reasonable range for drug candidates, since either low (<10 μM) or elevated aqueous solubility (>100 μM) can result in limited intestinal absorption [32]. Octanol/phosphate buffer (pH 7.4) partition coefficients (Log $D_{7.4}$) of 7–11 remained are within the ideal range for drug candidates, i.e., 2–3 [33,34].

Table 1. Physicochemical and *in vitro* pharmacokinetic properties of pyrazolamide derivatives.

Cpd	Aqueous Solubility ^(a) (μM)	Log $D_{7.4}$ ^(b)	PAMPA-GI ^(c)		PAMPA-BBB ^(d)		Plasma Metabolization Rate ^(e) (%)
			Pe Exp (10^{-6} cm/s)	Fa Exp (%)	Pe Exp (10^{-6} cm/s)	Score	
7	12.14	2.47	15.38	99.71	12.77	CNS+	56.13
8	59.07	1.94	9.69	97.49	17.25	CNS+	18.66
9	21.32	2.14	11.00	98.47	4.51	CNS+	24.56
10	47.66	2.43	2.51	61.51	12.68	CNS+	32.50
11	68.47	1.98	10.18	97.91	9.26	CNS+	13.04

^(a) Thermodynamic solubility determined by UV spectroscopy; ^(b) Determined by UV method after n-octanol/buffer partitioning at pH 7.4; ^(c) Soybean L- α -phosphatidylcholine was used as artificial lipid membrane in the wells of the donor plate; ^(d) Porcine brain lipid was used as artificial lipid membrane in the wells of the donor plate; ^(e) Determined after 240 min.

The membrane permeability of 7–11 measured using a gastrointestinal tract (GI) parallel artificial membrane permeability assay [35] (PAMPA) ranged from $2.5\text{--}15.3 \times 10^{-6}$ cm/s, which indicated excellent absorption rates (>60%) after oral administration of these substances (Table 1). In addition, considering that cannabinoid receptors are also expressed in the central nervous system [36], the PAMPA-BBB assay was also performed to determine the potential of these compounds to cross the blood–brain barrier [37,38] (Table 1). As expected, all the pyrazolamides had a permeability rate compatible with accessing the CNS (CNS+).

Although the results suggested elevated absorption of 7–11, clearance rates are also of concern for ideal bioavailability. Therefore, we also investigated the stability of 7–11 against enzymatic hydrolysis, as amide groups are potentially labile to plasma carboxylesterases [39] (Table 1). Flurbiprofen-derived pyrazolamides (8 and 11) showed increased stability against enzyme hydrolysis than corresponding ibuprofen-derived pyrazolamides (7 and 10), possibly by the steric effect of the bulkier and less flexible biphenyl system compared to 4-isobutylphenyl in the latter. The loss of ring coplanarity also contributes to the greater plasma stability of both 8 and 11, as the absence of the *ortho*-effect in 9 favors its metabolism, as shown in Table 1.

Furthermore, considering that the compounds developed in the present work have amide functional groups, the stabilities of the compounds were evaluated at gastric (pH 2) (Figure 3A) and plasmatic pH (7.4) (Figure 3B) to assess their susceptibility to pH-dependent chemical hydrolysis. After 240 min, derivatives 7–11 showed recovery rates of 70–100%, indicating the high chemical stability of these compounds at both pH values [40]. As expected, tertiary pyrazolamides 10 and 11 proved to be more resistant to hydrolysis than the corresponding secondary amides.

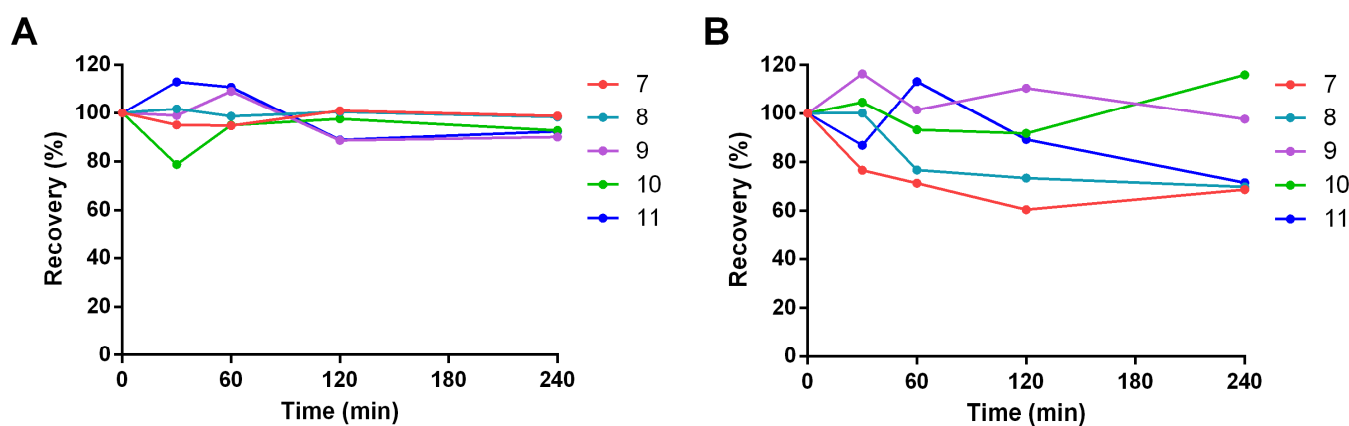


Figure 3. Chemical stability of compounds (7–11). (A) Chemical stability of compounds (7–11) at gastric pH (2.0). (B) Chemical stability of compounds (7–11) at plasma pH (7.4). Experiments were conducted in triplicate, and the values shown represent the averages from triplicate experiments.

Therefore, both absorption rates and chemical and plasma stability of 7–11 supported the possibility of their use by oral route, with flurbiprofen-derived pyrazolamides 8 and 11 presenting the best physicochemical (solubility, lipophilicity) and *in vitro* pharmacokinetic profile (permeability and stability) in comparison to the other analogs evaluated.

2.3. *In Vitro* Activity Profiles of Pyrazolamides 7–11

The agonist profile of pyrazolamides 7–11 towards cannabinoid receptors was investigated by measurement of cyclic AMP (cAMP) concentrations in CHO cells transfected with either human CB₁ or CB₂. The assay is based on receptor coupling to G proteins of the Gi/o family, whose activation results in adenylate cyclase inhibition and a decrease in intracellular cAMP [41–43]. When evaluated in CB₁-expressing cells, compounds 7–11 did not significantly alter the intracellular cAMP at either 1 μM or 10 μM [44], as the reduction in cAMP concentration did not exceed 25% of the maximum response obtained

with control agonist CP-55,940 (Figure 4 and Supplementary Material). Results indicate a concentration-dependent weak response and, although no structure-activity relationship was evidenced, these findings demonstrate that introduction of the methyl group in **10** and **11** did not result in a significant change in the activity profile of these compounds against CB₁ receptors compared to **7** and **8**, respectively.

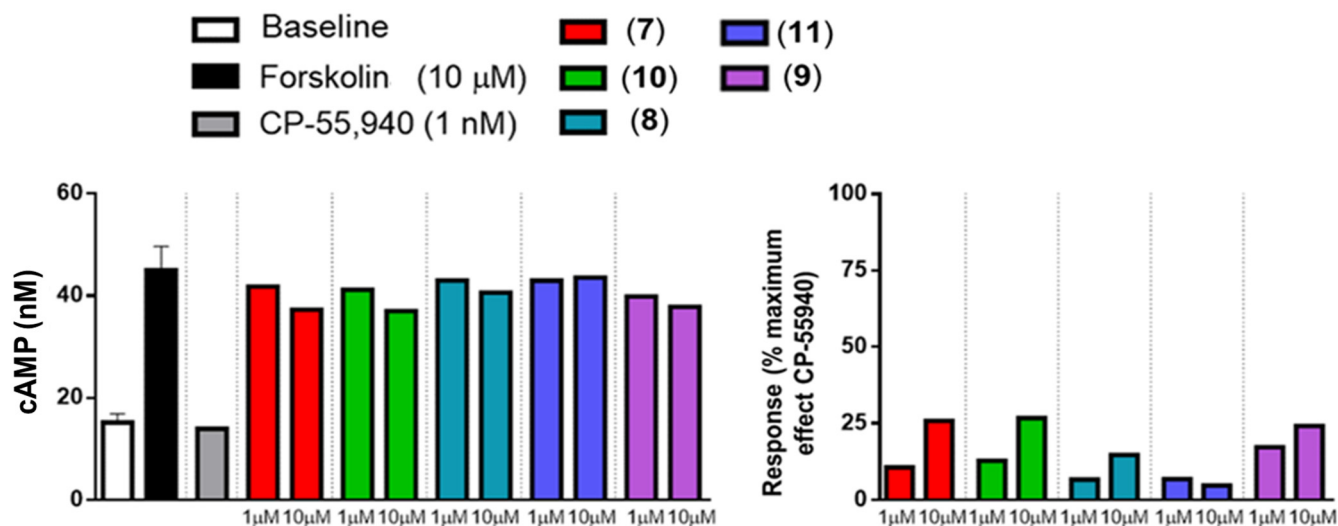


Figure 4. Effect of NSAID-pyrazolamides 7–11 on cyclic AMP intracellular concentration of CB₁-transfected CHO cells. Data represent results from single replicates.

On another hand, when evaluated in cells expressing human CB₂ receptors, compounds 7–11 showed a significant increase in cAMP concentrations when tested at 10 μM [44] (Figure 5). This result was in marked contrast with the response to 100 nM WIN 55212-2, which completely abolished the production of cAMP by forskolin, indicating a concentration-dependent inverse agonist profile for 7–11. Additionally, LASSBio-2265 (**11**) showed an important effect starting from 1 μM, while no effect was observed in CB₁-expressing cells.

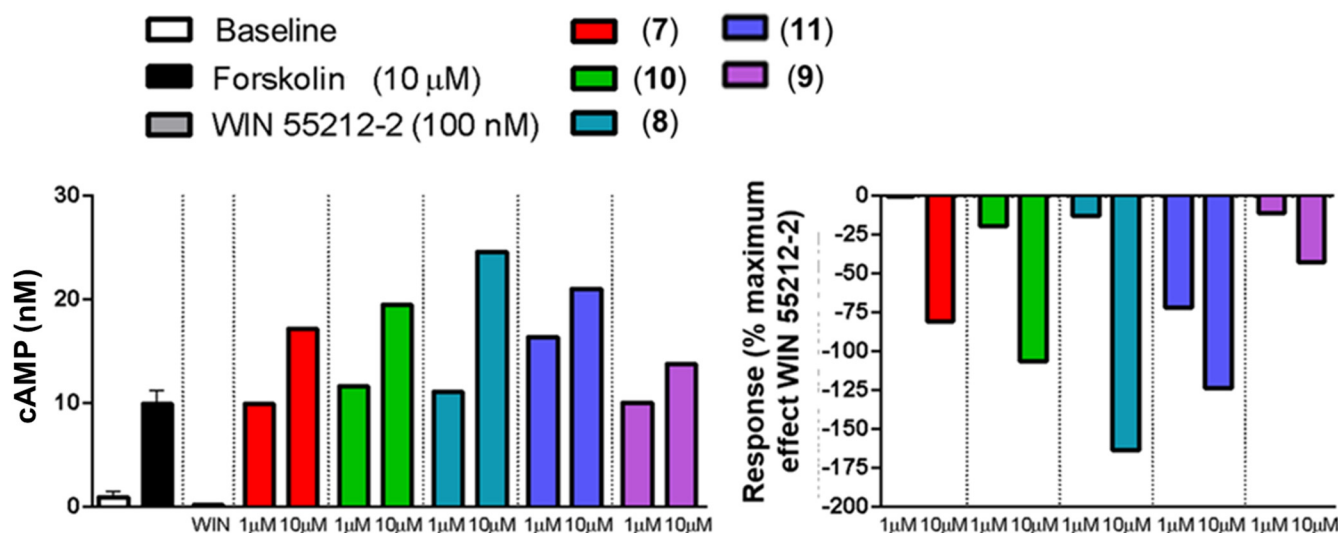


Figure 5. Effect of NSAID-pyrazolamides 7–11 on cyclic AMP intracellular concentration of CB₂-transfected CHO cells after stimulation with 10 μM forskolin. Data represent results from single replicates.

Considering the ensemble of results, LASSBio-2265 (**11**) was selected for further investigation to confirm the hypothesis of CB₂ inverse agonism. A concentration-response curve for the cAMP increase induced by compound **11** was assessed using chemiluminescent

detection in CHO-K1 CNR2 Gi cells stimulated with 8 μM (EC_{20}) forskolin, validated against full agonist CP 55,940 and inverse agonist SR 144,528 [45]. The functional status of the CB_2 receptor was monitored by cAMP quantification in relation to controls and it was possible to observe an increase in cAMP by DiscoverX HitHunter cAMP XS+ assay. The obtained data confirmed that LASSBio-2265 (**11**) is a partial inverse agonist of human CB_2 receptors, with an EC_{50} of $0.369 \pm 0.03 \mu\text{M}$ and an efficacy of 63% of the maximum effect.

Moreover, the binding affinity of LASSBio-2265 (**11**) to human CB_2 receptors was also studied to further confirm if the inverse agonist activity of LASSBio-2265 (**11**) was indeed product of an interaction with CB_2 receptors [46]. Competitive binding was evaluated in membranes from CB_2 -expressing CHO cells using [^3H]-WIN55212-2 as radioligand probe. The results indicated that **11** shows a moderate affinity for CB_2 receptors, with $\text{K}_i = 16.0 \pm 3 \mu\text{M}$. However, the affinity obtained for compound **11** is of similar magnitude to those found by Rogosch and coworkers for compounds **5** and **6**, as illustrated in Table 2. Potency and affinity values were determined from *in vitro* assays performed in duplicate.

Table 2. CB_2 receptor binding affinity of LASSBio-2265 (**11**) and arachidonyl-pyrazolamides (**5**) and (**6**).

Compound (μM)	K_i (μM)
(5)	5.4 ^(a)
(6)	3.0 ^(a)
LASSBio-2265 (11)	16.0

^(a) Data obtained from Rogosch and coworkers [20].

2.4. *In Vivo* Activity of LASSBio-2265 (**11**) in the Formalin-Induced Licking Response in Mice

Selective inverse agonists of CB_2 receptors, JTE-907 [47,48], SMM-189 [49], and Sch.414319 [50], have been indicated in the literature as beneficial agents for the treatment of diverse pathological conditions associated with inflammatory processes. Cascio and co-workers [51] described the antinociceptive activity of CB_2 receptor inverse agonists in the late phase of the classical formalin test, which induces a biphasic stereotypical nocifensive behaviour. Therefore, the analgesic profile of LASSBio-2265 (**11**) was evaluated in the same model (Figure 6), which measures nociceptive behavior after subcutaneous (s.c.) injection of dilute formalin (1.25% in saline, 30 μL) into one of the two hind paws of mice [52]. This assay presents two temporally distinct phases. The first (early) phase evokes nociception through the direct effect of formalin on the acute activation of pain-sensing C fibers at the peripheral endings of sensory neurons involved in pain transmission. After an interval of 10–15 min, a second, inflammatory-driven phase (late phase) of sustained pain behavior appears, in which sensory fiber activity is accompanied by inflammation and central sensitization [53].

In the first phase, only morphine (2.5 mg/kg) promoted significant analgesia compared to vehicle (5% DMSO in 0.9% NaCl), acetylsalicylic acid (ASA, 200 mg/kg) and LASSBio-2265 (**11**) at 1, 3 and 10 mg/kg. In contrast, during the second phase, LASSBio-2265 (**11**) proved to be comparable to both morphine and ASA, with dose-dependent progressive effect, thus proving to be promising for the treatment of conditions that lead to inflammatory pain. Naïve animals were evaluated in two phases of assay without any treatment (Figure 6).

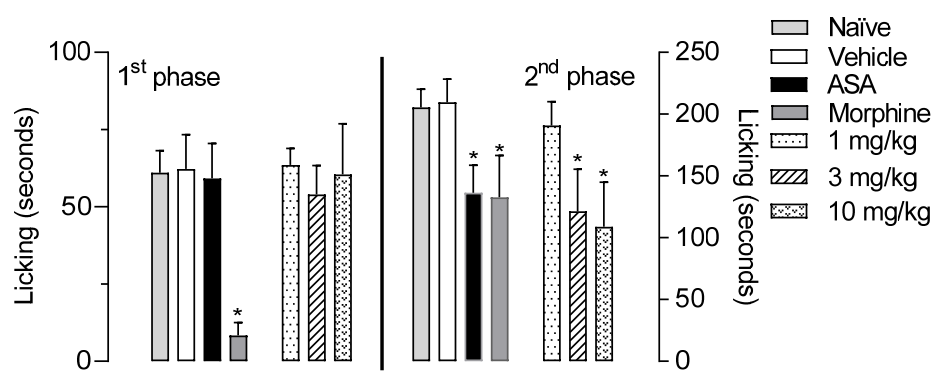


Figure 6. Antinociceptive effects of LASSBio-2265 (**11**) on formalin-induced licking behavior in mice. Mice were pretreated orally with LASSBio-2265 (**11**), morphine (2.5 mg/kg), acetylsalicylic acid (ASA, 200 mg/kg), or the vehicle, and the time spent licking the formalin-injected paw was recorded (in seconds) in the first phase (0–15 min post-formalin injection) and second phase (15–30 min post-formalin injection). The results are presented as the mean \pm SD ($n = 7$ mice per group). Statistical significance was calculated by one-way ANOVA followed by Tukey's test. * $p < 0.05$ compared with vehicle-treated mice.

3. Materials and Methods

3.1. Materials

Commercial reagents were obtained from Sigma–Aldrich (St. Louis, MI, USA). Melting points were determined by differential scanning calorimetry with a Shimadzu calorimeter (Model DSC-60). Fourier-transformed infrared (FTIR) spectra were obtained with Thermo-Scientific spectrometer (Model Nicolet iS10). ^1H - and ^{13}C -NMR spectra were obtained with VARIAN 400-MR and 500-MR spectrometers. High-performance liquid chromatography with detection by photodiode arrays (HPLC-PDA) was performed with Shimadzu LC20AD apparatus using a Kromasil 100-5C18 column (4.6 mm \times 250 mm) and SPD-M20A detector (Diode Variety). Ultraviolet-visible measurements were performed in a Femto scanning spectrophotometer (Model 800XI). High-resolution mass spectrometry (Orbitrap-HRMS) analysis was performed using a QExactive Hybrid Quadrupole Orbitrap Mass Spectrometer (Thermo Fisher Scientific, Waltham, MA, USA) with electrospray ionization (ESI) using solutions of the compounds (1 $\mu\text{g}/\text{mL}$) prepared in a 7:3 ratio of water:methanol fortified with 0.1% formic acid and 5 mM ammonium formate.

3.2. Synthesis of the NSAID-Pyrazolamides (7–11)

3.2.1. Synthesis of the NSAID-Pyrazolamides (7–9)

To a mixture of 0.95 mmol of carboxylic acid (**13**), (**14**), or (**15**), 185 mg (1.14 mmol, 1.2 eq.) of 1,1'-carbonyldiimidazole, 154 mg (1.14 mmol, 1.2 eq.) of hydroxybenzotriazole, and 260 μL (1.88 mmol, 2 eq.) of triethylamine, 290 mg (1.42 mmol, 1.5 eq.) of 4-amino-antipyrine (**3**) dissolved in 15 mL of dichloromethane was added. The reaction was magnetically stirred for 4 h at room temperature. After this time, the reaction mixture was poured into a separatory funnel and extracted with dichloromethane:water (2:3). The organic phase was treated with anhydrous sodium sulfate and concentrated under reduced pressure. The desired pyrazolamide (**7–9**) was obtained after purification by isocratic elution with ethyl acetate:hexane (9:1, v/v) from a flash silica gel column (1077341003; Millipore, Burlington, VT, USA), using approx. 1 g of silica per mg of raw product.

N-(1,5-dimethyl-3-oxo-2-phenyl-2,3-dihydro-1*H*-pyrazol-4-yl)-2-(4-isobutylphenyl) propanamide (**7**). White powder, 66% yield, m.p.: 151.2 $^{\circ}\text{C}$. ^1H -NMR (400 MHz, $\text{DMSO}-d_6$) δ (ppm): 9.18 (s, 1H); 7.5 (d, $J = 7.0$ Hz 2H); 7.4 (m, 2H); 7.31 (d, $J = 7.3$ Hz 2H), 7.10 (m, 3H); 7.08 (d, $J = 7.0$ Hz 2H), (s, 3 H); 3.82 (q, $J = 7.0$ Hz 1H); 3.00 (s, 1H); 2.41 (d, $J = 7.1$ Hz 2H); 1.97 (s, 3H); 1.81 (m, $J = 6.9$ Hz 1H); 1.36 (s, 1H); 0.86 (s, 3H); 0.84 (s, 3H). ^{13}C -NMR (100 MHz, $\text{DMSO}-d_6$) δ (ppm): 173.08 (C10); 161.80 (C15); 152.22 (C5); 139.36 (C2); 139.32

(C18); 135.05 (C21); 129.07 (C23, C25); 128.82 (C1, C3); 126.98 (C24); 126.16 (C4, C6); 123.39 (C22, C26); 44.39 (C14); 44.26 (C7); 36.06 44.39 (C9); 29.65 (C20); 22.20 (C8); 22.18 (C28, C29); 18.70 (C11); and 11.08 (C19). IR (ATR, cm^{-1}): 1682.06 (ν C=O); 3224.63 (ν N-H); and 2961.65 (ν C-H). ESI-FT-ICR, $[\text{M} + \text{H}]^+$ (calculated): 392.23325 m/z , $[\text{M} + \text{H}]^+$ (experimental): 392.23268 m/z .

N-(1,5-dimethyl-3-oxo-2-phenyl-2,3-dihydro-1*H*-pyrazol-4-yl)-2-(2-fluoro-[1,1'-biphenyl]-4-yl) propanamide (**8**). White powder, 66% yield, m.p.: 214.8 °C. $^1\text{H-NMR}$ (400 MHz, $\text{DMSO-}d_6$) δ (ppm): 9.35 (s, 1H); 7.54 (d, $J = 8.6$ Hz, 2H); 7.46 (m, 2H); 7.48 (d, $J = 7.1$ Hz, 2H); 7.36 (m, 1H); 7.4 (m, 1H); 7.31 (m, 3H); 3.93 (q, $J = 6.8$ Hz, 1H); 3.00 (s, 3H); 2.04 (s, 3H); and 1.43 (d, $J = 6.9$ Hz, 3H). $^{13}\text{C-NMR}$ (100 MHz, $\text{DMSO-}d_6$) δ (ppm): 172.37 (C14); 161.71 (C19); 157.85 (C3); 152.01 (C5); 135.01 (C7); 130.55 (C22); 130.52 (C22'); 129.06 (C25); 128.71 (C28); 128.69 (C28'); 128.60 (C27, C29); 127.74 (C9, C11); 126.20 (C10); 123.85 (C1); 123.44 (C8, C12); 114.98 (C26, C30); 114.79 (C18); 107.41 (C6); 44.24 (C13); 36.03 (C24); 18.54 (C15) and 11.22 (C23). IR (ATR, cm^{-1}): 1680.78 (ν C=O amide); and 3196.11 (ν N-H). ESI-FT-ICR, $[\text{M} + \text{H}]^+$ (calculated): 430.19253 m/z , $[\text{M} + \text{H}]^+$ (experimental): 430.19174 m/z .

2-([1,1'-biphenyl]-4-yl)-*N*-(1,5-dimethyl-3-oxo-2-phenyl-2,3-dihydro-1*H*-pyrazol-4-yl) acetamide (**9**). Yellow powder, 56% yield, m.p.: 221.8 °C. $^1\text{H-NMR}$ (400 MHz, $\text{DMSO-}d_6$) δ (ppm): 9.35 (s, 1H); 7.66 (m, 2H); 7.62 (m, 2H); 7.51 (d, $J = 7.7$ Hz, 2H); 7.47 (s, 1H); 7.42 (m, 2H); 7.35 (t, $J = 7.4$ Hz, 1H); 7.3 (m, 3H); 3.65 (s, 2H); 3.03 (s, 3H); and 2.07 (s, 3H). $^{13}\text{C-NMR}$ (100 MHz, $\text{DMSO-}d_6$) δ (ppm): 169.73 (C14); 161.81 (C18'); 152.25 (C2); 129.39 (C5); 129.38 (C21); 129.34 (C24); 129.33 (C26, C28); 129.19 (C9, C11); 128.74 (C27); 128.73 (C4, C6); 126.77 (C10); 126.38 (C8, C12); 107.52 (C1, C3); 41.68 (C25, C29); 35.78 (C17); 11.33 (C13) and 11.17 (C23). IR (ATR, cm^{-1}): 1680.29 (ν C=O) and 3304.28 (ν N-H). ESI-FT-ICR, $[\text{M} + \text{H}]^+$ (calculated): 398.18630 m/z , $[\text{M} + \text{H}]^+$ (experimental): 398.18582 m/z .

3.2.2. Synthesis of *N*-Methylated Pyrazolamides (**10**) and (**11**)

To a round-bottomed balloon containing 0.25 mmol of compound (**7**) or (**8**), 1.5 eq. of sodium hydride (from a 60% dispersion in mineral oil dissolved in 5 mL of anhydrous tetrahydrofuran) was added under an argon atmosphere. After 15 min at 0 °C, 47 μL (0.75 mmol, 3 eq.) iodomethane was added, and the reaction was monitored by TLC until completion (aprox. 4 h). The reaction mixture was poured into a separatory funnel and extracted with dichloromethane:water (2:3). The organic phase was treated with anhydrous sodium sulfate and concentrated under reduced pressure. The desired pyrazolamide (**10** or **11**) was obtained after purification by isocratic elution with ethyl acetate:hexane (9:1, v/v) from a flash silica gel column (1077341003; Millipore, USA), using aprox. 1 g of silica per mg of raw product [28].

N-(1,5-dimethyl-3-oxo-2-phenyl-2,3-dihydro-1*H*-pyrazol-4-yl)-2-(4-isobutylphenyl)-*N*-methylpropanamide (**10**). Yellow oil. $^1\text{H-NMR}$ (400 MHz, $\text{DMSO-}d_6$) δ (ppm): 7.57 (s, 1H); 7.55 (s, 1H); 7.53 (d, $J = 8.6$ Hz, 2H); 7.39 (d, $J = 7.3$ Hz, 2H); 7.09 (s, 1H); 7.07 (s, 1H); 6.89 (d, $J = 7.0$ Hz 1H); 3.72 (q, $J = 6.7$ Hz, 1H, H2); 2.97 (s, 3H); 2.95 (s, 3H); 2.40 (d, $J = 7.0$ Hz, 2H); 1.80 (m, 1H); 1.33 (s, 3H); 1.20 (d, $J = 6.8$ Hz, 3H); and 0.87 and 0.85 (s, 3H). $^{13}\text{C-NMR}$ (100 MHz, $\text{DMSO-}d_6$) δ (ppm): 174.36 (C10); 161.39 (C15); 153.53 (C5); 139.73 (C2); 134.76 (C18); 129.21 (C21); 129.12 (C1, C3); 129.00 (C23, C25); 126.80 (C24); 124.19 (C14); 112.61 (C22, C26); 44.26 (C7); 42.92 (C9); 35.94 (C20'); 35.02 (C30); 29.63 (C8); 22.10 (C28, C29); 20.51 (C11); and 9.13 (C19). IR (ATR, cm^{-1}): 1655.36 (ν C=O) and 2925.59 and 2956.95 (ν C-H). ESI-FT-ICR, $[\text{M} + \text{H}]^+$ (calculated): 406.24890 m/z , $[\text{M} + \text{H}]^+$ (experimental): 406.24832 m/z .

N-(1,5-dimethyl-3-oxo-2-phenyl-2,3-dihydro-1*H*-pyrazol-4-yl)-2-(2-fluoro-[1,1'-biphenyl]-4-yl)-*N*-methylpropanamide (LASSBio-2265) (**11**). Yellow oil. $^1\text{H-NMR}$ (500 MHz, CDCl_3) δ (ppm): signals unfolded due to the presence of 2 rotamers (approximate 4:1 ratio) 7.5 (m, 2H); 7.37 (m, 3H); 7.34 (m, 2H); 6.98 (m, 1H); 6.90 (m, 3H); 6.85 (m, 3H) 3.80 (q, $J = 7.0$ Hz, 1H, minor); 3.72 (q, $J = 6.9$ Hz, 1H, major); 3.14 (s, 3H); 3.00 (s, 1H); 1.45 (s, 3H, major); 1.42 (s, 3H, minor); 1.26 (d, 1H); and 1.23 (d, 1H). $^{13}\text{C-NMR}$ (100 MHz, acetonitrile- d_3) δ (ppm): 175.50 (C14); 163.01 (C3); 161.67 (C19); 159.24 (C5); 154.57 (C22); 131.99 (C7); 130.25 (25); 129.94 (C28); 129.91 (C28'); 129.59 (C27, C29); 128.84 (C9, C11);

128.13 (C10); 125.65 (C18); 124.75 (C8, C12); 115.82 (C1); 115.59 (C26, C30); 113.83 (C6); 44.38 (C13); 36.81 (C24); 35.90 (C33); 20.58 (C15) and 10.15 (C23). IR (ATR, cm^{-1}): 1665.03 (ν C=O) and 2980.12 and 2932.32 (ν C-H). ESI-FT-ICR, $[\text{M} + \text{H}]^+$ (calculated): 444.20818 m/z , $[\text{M} + \text{H}]^+$ (experimental): 444.20806 m/z .

Structural characterization of pyrazolamide (7–11) is shown in Figures S1–S28.

3.3. Drug-like Properties of NSAID-Pyrazolamides (7–11)

3.3.1. Aqueous Solubility

The test was performed based on the absorbance obtained by ultraviolet spectroscopy. The scanning wavelength was determined according to the highest absorbance observed for each compound. Saturated aqueous solution of the analyzed compounds were stirred for 4 h at 37 °C, and then filtered through a 0.45 μm PVDF filter and transferred to a quartz cuvette (10 mm optical path) for reading. Solubility was determined by linear regression based on the equation of the line [31].

3.3.2. Determination of the Distribution Coefficient at pH 7.4 ($\log D_{7.4}$)

The assay was performed based on the shake-flask method and the absorbance readings by ultraviolet spectroscopy at maximum absorbance wavelength. To a Falcon tube with a capacity of 15 mL, 5 mL of buffer solution at pH 7.4 and 5 mL of 1-octanol were added. Then, the tested compounds were added at defined concentrations of approximately 10–15 μM , and the mixtures were homogenized via vigorous manual shaking. Next, the Falcon tubes were stirred for 4 h at 37 °C, and the experiment was carried out in triplicate for each compound. Subsequently, each sample was placed in a separatory funnel, and the collected aqueous phase was filtered through a 0.45 μm PVDF filter and transferred to a quartz cuvette (10 mm optical path) for UV/Vis reading. The distribution coefficient of each compound at pH 7.4 was determined by linear regression using the straight-line equation [33].

3.3.3. Chemical Stability

To a 2 mL microtube, 2 μL of a 5 mM concentrated solution of the analyzed compound (solubilized in DMSO) and 248 μL of acid buffer (0.2 M potassium chloride and 0.2 M HCl; pH = 2) or neutral (dibasic phosphate; pH = 7.4) were added. The experiment was carried out in triplicate. After vortexing, the mixture was placed in a water bath at 37 °C under vigorous stirring for 0, 30, 60, 120, and 240 min. After each reaction time, 248 μL of basic buffer (phosphate buffer, pH = 7.4) was added to neutralize the pH of the medium in the experiments using acidic buffer (pH = 2). Extraction of the compound was carried out by adding 1 mL of acetonitrile. The entire contents of the microtube were vortexed vigorously, and the container was placed in a freezer (−20 °C) to freeze the aqueous phase. Then, the organic phase was separated, filtered through an HPLC filter with a 0.45 μm PVDF membrane of 25 mm in diameter, and analyzed by HPLC-PDA (mobile phase: acetonitrile:water 60:40). The injection volume of the samples was 20 μL at a flow rate of 1.0 mL/min. Quantitation was performed at 272 nm for compounds (7), (8), and (10), 247 nm for compound (8) and LASSBio-2265 (11), and 253 nm for compound (9) [40].

3.3.4. Parallel Artificial Membrane Permeability Assay (PAMPA-GTI)

A 10 mM solution of each compound (tests and controls) was prepared in DMSO. Then, in a 5 mL glass flask, 250 μL of the freshly prepared solution was homogenized with 4750 μL of PBS at pH 6.6 to a concentration of 10 mM. The solution was then filtered in a 0.45 μm PVDF filter and set aside. Then, 180 μL of a solution of phosphate-buffered saline (PBS, pH 7.4):DMSO (95:5) was added to the wells of the receptor plate, and 5 μL of the soy L- α -phosphatidylcholine lipid solution (20 mg/mL in dodecane) was added to the wells of the donor plate. After 5 min, the donor plate received 180 μL of the reserved solution containing each compound. Afterward, the donor plate was carefully placed on top of the recipient, and the plates were agitated at 50 rpm for 8 h at room temperature (± 25 °C) in

a closed container containing 10 mL of PBS at pH 7.4. After this period, the donor plate was removed, and the contents of the recipient plate were transferred to a UV reading plate and read (SpectraMax 5, Molecular Devices) at the maximum wavelengths for each compound. The blank was prepared with 180 μ L of PBS solution (pH 7.4):DMSO (95:5). The experiments were carried out in triplicate with two different analyses ($n = 2$) [37]. The optical density values obtained from the readings at each selected wavelength for each of the compounds were analyzed by comparison with the values of the controls. These values were used to determine the absorbed fraction (Fa %) using the JMP[®] program version 10.0. The permeability results from PAMPA-TGI [35,54] classified the compounds according to the absorbed fraction percentage (Fa%) as follows: high intestinal permeability: >70%; medium intestinal permeability: 30–69%; or low intestinal permeability: <29% [55].

3.3.5. Parallel Artificial Membrane Permeability Assay (PAMPA-BBB)

In a 5 mL glass vial, 1 mg of each compound (test or control) was dissolved in 1 mL of ethanol. Then, 500 μ L of ethanol and 3.5 mL of PBS at pH 7.4 were added to this solution. The solution was then filtered in a 0.45 μ m PVDF filter and set aside. Subsequently, 180 μ L of a solution of PBS (pH 7.4): ethanol (70:30) was added to the wells of the receptor plate, and 5 μ L of porcine brain lipid solution (20 mg/mL in dodecane) was added to the wells of the donor plate. After 5 min, the donor plate received 180 μ L of each compound solution in triplicate. Then, the donor plate was carefully placed on top of the recipient plate, forming a sandwich system, and the plates were left to rest for 2 h and 45 min at room temperature (± 25 °C) in a closed container containing 10 mL of PBS at pH 7.4. After this period, the donor plate was removed, and the contents of the recipient plate were transferred to a UV reading plate and read (SpectraMax 5, Molecular Devices) at the maximum wavelengths for each compound. The blank was prepared with 180 μ L of PBS solution (pH 7.4):ethanol (70:30) [56]. The experiments were performed in triplicate with two different analyses ($n = 2$). Assay validation was performed using atenolol, caffeine, diazepam, enoxacin, ofloxacin, testosterone, and verapamil, which are reference compounds with described permeability values and were used as standards. Results indicated (a) CNS+ (high predicted BBB permeability) $Pe > 4.0 \times 10^{-6}$ cm/s; (b) CNS– (low predicted BBB permeability) $Pe < 2.0 \times 10^{-6}$ cm/s; and (c) CNS+ / – (uncertain permeability) Pe between 2.0 – 4.0×10^{-6} cm/s [56,57].

3.3.6. Plasmatic Stability

For the evaluation of plasma stability against plasma carboxylesterases, a pool of plasma male Wistar rats weighing 300–360 g kept in the vivarium of the Laboratory of Biochemical and Molecular Pharmacology-UFRJ was used. Blood was collected with heparin and kept on ice. Then, the samples were centrifuged at 2000 rpm for 15 min at 20 °C, with subsequent removal of the plasma. The plasma was then diluted 80% (v/v) with phosphate buffer (PBS; pH = 7.4) at 37 °C. The experiments performed in this work were approved by the Ethics Committee on the Use of Animals in Scientific Experiments of the Health Sciences Center of the Federal University of Rio de Janeiro (Number 028/15). The biological matrix was incubated at 37 °C under agitation for 30, 60, 120, and 240 min. The degree of degradation was evaluated by HPLC-PDA with methyl 1,1'-bisphenyl-4-carboxylate as an internal standard (PI), using an isocratic mobile phase of 70%:30% acetonitrile:water (0–15 min), an injection volume of 20 μ L, a flow rate of 1 mL/min, and detection at 254 nm [39].

3.4. In Vitro Experiments

3.4.1. Agonist Activity toward CB1 and CB2 Receptors

The cellular functional assay used to evaluate the agonist activity of planned pyrazolamides (7–11) toward cannabinoid receptor subtypes 1 and 2 was carried out at Eurofins Discovery France (<https://www.eurofinsdiscoveryservices.com/>) under the study number 100050410 (accessed on 28 October 2019) using the protocol previously published by Felder

and coworkers [44]. Briefly, pyrazolamides 7–11 were assayed at concentrations of 1 μ M and 10 μ M to evaluate their ability to change intracellular cAMP in CHO cells transfected with human CB₁ and CB₂ receptors [44], for 30 or 10 min at 37 °C after stimulation with 10 μ M forskolin, respectively. Negative and blank controls were performed in triplicate with and without the addition of forskolin, respectively. Positive controls used were CB agonists CP-55,940 (at 1 nM) and WIN 55,212-2 (at 100 nM).

3.4.2. Inverse Agonist Activity toward CB₂ Receptors [45]

The cellular functional assay used to evaluate the inverse agonist activity of LASSBio-2265 (11) toward the cannabinoid CB₂ receptor was carried out at Eurofins DiscoveryX Corporation USA (<https://www.discoverx.com/home>) under the study number FR095-0025341-Q (accessed on 02 June 2021) using the GPCR Biosensor Assay. Cell line cAMP Hunter CHO-K1 CNR2 Gi was seeded at a total volume of 20 μ L into white-walled, 384-well microplates and incubated at 37 °C prior to testing in the presence of 8 μ M (EC₂₀) forskolin. The media was aspirated from the cells and replaced with 15 μ L a 2:1 solution of Hanks' balanced salt solution (HBSS)/10 mM Hepes:cAMP XS+ Ab reagent. Intermediate dilution of the sample stocks was performed to generate 4 \times samples in assay buffer containing 32 μ M forskolin. Then, 5 μ L of each 4 \times sample was added to the cells and incubated at 37 °C for 60 min. The final assay vehicle concentration was 1%. After incubation, the assay signal was generated by incubation with 20 μ L cAMP XS+ ED/CL lysis cocktail for 1 h followed by incubation with 20 μ L cAMP XS+ EA reagent for 3 h at room temperature. After signal generation, the microplates were read with a PerkinElmer Envision instrument for chemiluminescent signal detection. Compound activity was analyzed using the CBIS data analysis suite (ChemInnovation, San Diego, CA, USA). Percent activity was calculated using the following formula:

$$\% \text{ Inverse Agonist Activity} = 100\% \times ((\text{mean RLU of test sample} - \text{mean RLU of EC}_{20} \text{ forskolin}) / (\text{mean RLU of forskolin positive control} - \text{mean RLU of EC}_{20} \text{ control})).$$

Data obtained from duplicate experiments were fit to concentration-response curves by non-linear regression of the Hill equation. Curve-fit parameters and standard errors were calculated using GraphPad Prism 6.0 (Hercules, CA, USA).

3.4.3. Human CB₂ (Agonist Radioligand) Receptor Binding Assay

Assays of binding to CB₂ receptors were performed at Eurofins Discovery France (<https://www.eurofinsdiscoveryservices.com/>) under the study number 100057099 (accessed on 3 June 2021) using the protocol previously published by Munro, Thomas, and Abu-Shaar [46]. Human recombinant CB₂ receptors were expressed in CHO cells, and binding was performed with [³H]-WIN 55212-2, which is a nonselective agonist radioligand. The analysis was performed using software developed at Cerep (Hill software, Santa Barbara, CA, USA) and SigmaPlot 4.0 for Windows (©1997 by SPSS Inc., Chicago, IL, USA).

Data obtained from duplicate experiments were fit to concentration-response curves by non-linear regression of the Hill equation. Curve-fit parameters and standard errors were calculated using GraphPad Prism 6.0 (Hercules, CA, USA).

3.5. In Vivo Experiments

3.5.1. Animals

Swiss Webster mice (20–25 g, 30–40 days old), from both sexes were donated by the Instituto Vital Brazil (Niteroi, Rio de Janeiro, Brazil). The mice were maintained in a room with a 12 h light-dark cycle at 22 \pm 2 °C and 60% to 80% humidity, with food and water provided *ad libitum*. The mice were acclimatized to the laboratory conditions for at least 1 h before each test onset and were used only once throughout the experiments. All protocols were conducted in accordance with the Guidelines on Ethical Standards for Investigation of Experimental Pain in Mice (Zimmermann, 1983) and followed the principles and guidelines adopted by the National Council for the Control of Animal Experimentation (CONCEA) approved by the Ethical Committee for Animal Research (CEUA, approval in 30 April 2019,

receiving the number 31/19). All experimental protocols were performed during the light phase. The animal numbers per group were kept to a minimum, and at the end of each experiment, the mice were euthanized by ketamine/xylazine overdose.

3.5.2. Formalin-Induced Licking Behavior

This assay was performed as described by Hunskaar et al. [53] and adapted by Gomes et al. [58]. This model was characterized by a response that occurred in two phases. The first phase (acute neurogenic pain) occurred during the first 5 min after the intraplantar injection of formalin, and the second phase (inflammatory pain) occurred 15 to 30 min post-injection. Mice were pretreated with oral doses of LASSBio-2265 (**11**, at 1, 3 or 10 mg/kg, p.o.), morphine (2.5 mg/kg, i.p.), acetylsalicylic acid (ASA, 200 mg/kg, p.o.), or the vehicle (same amount of DMSO used to solubilize the substances + NaCl 0.9%) 60 min before the administration of formalin. The naïve group was composed of animals that did not receive any oral treatment. Then, mice (n = 7 per group) received 20 µL of formalin (2.5% v/v) in the dorsal surface of the left hind paw. The time that the mice spent licking the injected paw was immediately recorded. The amount of DMSO used did not affect or interfere per se with the experimental model. The final volume administered to mice was 0.1 mL. The protocol was carried out by a blinded experimenter that did not know the drug treatment conditions and groups.

4. Conclusions

NSAID-pyrazolamides **7–11** were obtained in good yields from classical synthetic methodologies. All compounds presented adequate aqueous solubility, lipophilicity, permeability, and stability to chemical and enzymatic hydrolysis for the development of orally administered drug candidates. Compounds **7–11** also showed high permeability through artificial membranes mimicking the blood–brain barrier, as cannabinoid receptors are widely distributed in the central nervous system. Their stability against carboxylesterases also reinforces that observed effects are not resulting from the effect of precursors, i.e., 4-aminoantipyrine and NSAID. The chemical stability of pyrazolamides **7–11** indicated that the compounds are highly stable and are not susceptible to pH-dependent hydrolysis, unlike dipyrone.

The *in vitro* experiments performed for characterization of the intrinsic efficacy of LASSBio-2265 (**11**) in CB₂ receptors showed a moderate ligand profile (K_i = 16 µM) with EC₅₀ = 0.36 µM (E_{max} = 63%) in CHO cells. For *in vivo* studies, antinociceptive effects of **11** were demonstrated by decreased pain behaviour in the formalin test in mice at 3 mg/kg, suggesting that it could be a promising candidate for the treatment of pain syndromes associated with chronic inflammatory diseases.

Supplementary Materials: The following supporting information can be downloaded at: <https://www.mdpi.com/article/10.3390/ph15121519/s1>, Figures S1–S6: Structural characterization of pyrazolamide (**7**); Figures S7–S12: Structural characterization of pyrazolamide (**8**); Figures S13–S18: Structural characterization of pyrazolamide (**9**); Figures S19–S23: Structural characterization of pyrazolamide (**10**); Figures S24–S28: Structural characterization of pyrazolamide (**11**); Figures S29 and S30: Structural characterization of bismethylated pyrazolamide (**16**); Figures S31 and S32: Alternative methodology tried for the synthesis pyrazolamide (**12**); Figure S33: Calibration curves for determination of aqueous solubility of the pyrazolamides (**7–11**); Figure S34: pH-Dependent chemical stability of pyrazolamides (**7–11**); Figure S35–S36: Absorbed fraction of drugs used as standard of GIT and BBB-PAMPA model and pyrazolamides (**7–11**); Figure S37–S39: Plasma stability profile of pyrazolamides (**7–11**); Figure S40: Dose-response curve of inverse agonism for cannabinoid receptor 2 (CB₂) performed by the company Eurofins-CEREP: (A) control inverse agonist SR 144528 and (B) LASSBio-2265 (**11**); Table S1: Absorbed fraction of drugs used as standard and pyrazolamides (**7–11**) determined in the PAMPA-GTI model; Table S2: Permeability of drugs used as standard, and pyrazolamides (**7–11**) determined in the PAMPA- BBB model; Table S3: Evaluation the agonist effect against the CB₁ receptors of the pyrazolamides (**7–11**); Table S4: Evaluation the agonist effect against

the CB2 receptors of the pyrazolamides (7–11); Table S5: Raw data from the inverse agonism assay performed by the company Eurofins-CEREP.

Author Contributions: Conceptualization, C.A.M.F., R.C.M., D.R.d.O.; methodology, D.R.d.O., R.C.M., G.B., P.R.d.C.F.; validation, D.R.d.O., G.B., P.R.d.C.F.; formal analysis, D.R.d.O., G.B., P.R.d.C.F.; investigation, D.R.d.O., G.B., P.R.d.C.F.; resources, C.A.M.F., L.M.L., P.D.F.; writing—original draft preparation, D.R.d.O., P.R.d.C.F.; writing—review and editing, C.A.M.F., L.M.L., P.D.F.; visualization, D.R.d.O., G.B., P.R.d.C.F.; supervision, C.A.M.F., L.M.L., P.D.F.; project administration, C.A.M.F., R.C.M., D.R.d.O.; funding acquisition, C.A.M.F., P.D.F., P.R.d.C.F. All authors have read and agreed to the published version of the manuscript.

Funding: This study was financed in part by the Coordenação de Aperfeiçoamento de Pessoal de Nível Superior—Brasil (CAPES)—Finance Code 001. The authors would like to thank INCT-INOVAR (BR, grant number 465.249/2014-0), Fundação Carlos Chagas Filho de Amparo à Pesquisa do Estado do Rio de Janeiro (FAPERJ, grant numbers E-26/010.001273/2016; E-26/202.878/2018 and SEI-260003/003613/2022, fellowship to CAMF; E-26/202.763/2018 and SEI-260003/001182/2020, fellowship to PRCF), Conselho Nacional de Desenvolvimento Científico e Tecnológico (CNPq, grant number 304394/2017-3). We would like to thank Alan Minho for technical assistance and the Instituto Vital Brazil (Niterói, Brazil) for donation of mice.

Institutional Review Board Statement: The animal study protocol was approved by the Ethical Committee for Animal Research (CEUA, approval in 30 April 2019, receiving the number no. 31/19).

Informed Consent Statement: Not applicable.

Data Availability Statement: Not applicable.

Conflicts of Interest: The authors declare no conflict of interest.

References

1. Guindon, J.; Hohmann, A. The Endocannabinoid System and Pain. *CNS Neurol. Disord.-Drug Targets* **2009**, *8*, 403–421. [[CrossRef](#)]
2. Curto-Reyes, V.; Llamas, S.; Hidalgo, A.; Menéndez, L.; Baamonde, A. Spinal and Peripheral Analgesic Effects of the CB₂ Cannabinoid Receptor Agonist AM1241 in Two Models of Bone Cancer-Induced Pain. *Br. J. Pharmacol.* **2010**, *160*, 561–573. [[CrossRef](#)] [[PubMed](#)]
3. Hama, A.; Sagen, J. Centrally Mediated Antinociceptive Effects of Cannabinoid Receptor Ligands in Rat Models of Nociception. *Pharmacol. Biochem. Behav.* **2011**, *100*, 340–346. [[CrossRef](#)] [[PubMed](#)]
4. Beaulieu, P.; Bisogno, T.; Punwar, S.; Farquhar-Smith, W.P.; Ambrosino, G.; Di Marzo, V.; Rice, A.S. Role of the Endogenous Cannabinoid System in the Formalin Test of Persistent Pain in the Rat. *Eur. J. Pharmacol.* **2000**, *396*, 85–92. [[CrossRef](#)] [[PubMed](#)]
5. Finn, D.P.; Jhaveri, M.D.; Beckett, S.R.G.; Roe, C.H.; Kendall, D.A.; Marsden, C.A.; Chapman, V. Effects of Direct Periaqueductal Grey Administration of a Cannabinoid Receptor Agonist on Nociceptive and Aversive Responses in Rats. *Neuropharmacology* **2003**, *45*, 594–604. [[CrossRef](#)]
6. Maione, S.; Bisogno, T.; de Novellis, V.; Palazzo, E.; Cristino, L.; Valenti, M.; Petrosino, S.; Guglielmotti, V.; Rossi, F.; Marzo, V. Di Elevation of Endocannabinoid Levels in the Ventrolateral Periaqueductal Grey through Inhibition of Fatty Acid Amide Hydrolase Affects Descending Nociceptive Pathways via Both Cannabinoid Receptor Type 1 and Transient Receptor Potential Vanilloid Type-1 Re. *J. Pharmacol. Exp. Ther.* **2006**, *316*, 969–982. [[CrossRef](#)] [[PubMed](#)]
7. Rahn, E.J.; Hohmann, A.G. Cannabinoids as Pharmacotherapies for Neuropathic Pain: From the Bench to the Bedside. *Neurotherapeutics* **2009**, *6*, 713–737. [[CrossRef](#)] [[PubMed](#)]
8. Burgos, E.; Pascual, D.; Martín, M.I.; Goicoechea, C. Antinociceptive Effect of the Cannabinoid Agonist, WIN 55,212-2, in the Orofacial and Temporomandibular Formalin Tests. *Eur. J. Pain* **2010**, *14*, 40–48. [[CrossRef](#)] [[PubMed](#)]
9. Kinsey, S.G.; Mahadevan, A.; Zhao, B.; Sun, H.; Naidu, P.S.; Razdan, R.K.; Selley, D.E.; Imad Damaj, M.; Lichtman, A.H. The CB₂ Cannabinoid Receptor-Selective Agonist O-3223 Reduces Pain and Inflammation without Apparent Cannabinoid Behavioral Effects. *Neuropharmacology* **2011**, *60*, 244–251. [[CrossRef](#)] [[PubMed](#)]
10. Cumella, J.; Hernández-Folgado, L.; Girón, R.; Sánchez, E.; Morales, P.; Hurst, D.P.; Gómez-Cañas, M.; Gómez-Ruiz, M.; Pinto, D.C.G.A.; Goya, P.; et al. Chromenopyrazoles: Non-Psychoactive and Selective CB₁ Cannabinoid Agonists with Peripheral Antinociceptive Properties. *ChemMedChem* **2012**, *7*, 452–463. [[CrossRef](#)] [[PubMed](#)]
11. Martin, B.R.; Compton, D.R.; Thomas, B.F.; Prescott, W.R.; Little, P.J.; Razdan, R.K.; Johnson, M.R.; Melvin, L.S.; Mechoulam, R.; Susan, J.W. Behavioral, Biochemical, and Molecular Modeling Evaluations of Cannabinoid Analogs. *Pharmacol. Biochem. Behav.* **1991**, *40*, 471–478. [[CrossRef](#)] [[PubMed](#)]
12. Moreira, F.A.; Grieb, M.; Lutz, B. Central Side-Effects of Therapies Based on CB₁ Cannabinoid Receptor Agonists and Antagonists: Focus on Anxiety and Depression. *Best Pract. Res. Clin. Endocrinol. Metab.* **2009**, *23*, 133–144. [[CrossRef](#)]

13. Guindon, J.; Hohmann, A.G. Cannabinoid CB 2 Receptors: A Therapeutic Target for the Treatment of Inflammatory and Neuropathic Pain. *Br. J. Pharmacol.* **2008**, *153*, 319–334. [[CrossRef](#)] [[PubMed](#)]
14. Ahn, K.; Johnson, D.S.; Mileni, M.; Beidler, D.; Long, J.Z.; McKinney, M.K.; Weerapana, E.; Sadagopan, N.; Liimatta, M.; Smith, S.E.; et al. Discovery and Characterization of a Highly Selective FAAH Inhibitor That Reduces Inflammatory Pain. *Chem. Biol.* **2009**, *16*, 411–420. [[CrossRef](#)]
15. Comelli, F.; Giagnoni, G.; Bettoni, I.; Colleoni, M.; Costa, B. The Inhibition of Monoacylglycerol Lipase by URB602 Showed an Anti-Inflammatory and Anti-Nociceptive Effect in a Murine Model of Acute Inflammation. *Br. J. Pharmacol.* **2009**, *152*, 787–794. [[CrossRef](#)] [[PubMed](#)]
16. Guindon, J.; Desroches, J.; Beaulieu, P. The Antinociceptive Effects of Intraplantar Injections of 2-Arachidonoyl Glycerol Are Mediated by Cannabinoid CB 2 Receptors. *Br. J. Pharmacol.* **2007**, *150*, 693–701. [[CrossRef](#)] [[PubMed](#)]
17. Naidu, P.S.; Kinsey, S.G.; Guo, T.L.; Cravatt, B.F.; Lichtman, A.H. Regulation of Inflammatory Pain by Inhibition of Fatty Acid Amide Hydrolase. *J. Pharmacol. Exp. Ther.* **2010**, *334*, 182–190. [[CrossRef](#)] [[PubMed](#)]
18. Turcotte, C.; Chouinard, F.; Lefebvre, J.S.; Flamand, N. Regulation of Inflammation by Cannabinoids, the Endocannabinoids 2-Arachidonoyl-Glycerol and Arachidonoyl-Ethanolamide, and Their Metabolites. *J. Leukoc. Biol.* **2015**, *97*, 1049–1070. [[CrossRef](#)]
19. Hinz, B.; Cheremina, O.; Bachmakov, J.; Renner, B.; Zolk, O.; Fromm, M.F.; Brune, K. Dipyrrone Elicits Substantial Inhibition of Peripheral Cyclooxygenases in Humans: New Insights into the Pharmacology of an Old Analgesic. *FASEB J.* **2007**, *21*, 2343–2351. [[CrossRef](#)]
20. Rogosch, T.; Sinning, C.; Podlewski, A.; Watzer, B.; Schlosburg, J.; Lichtman, A.H.; Cascio, M.G.; Bisogno, T.; Di Marzo, V.; Nüsing, R.; et al. Novel Bioactive Metabolites of Dipyrrone (Metamizol). *Bioorg. Med. Chem.* **2012**, *20*, 101–107. [[CrossRef](#)] [[PubMed](#)]
21. Schenk, S.A.; Dick, F.; Herzog, C.; Eberhardt, M.J.; Leffler, A. Active Metabolites of Dipyrrone Induce a Redox-Dependent Activation of the Ion Channels TRPA1 and TRPV1. *Pain Rep.* **2019**, *4*, e720. [[CrossRef](#)] [[PubMed](#)]
22. Escobar, W.; Ramirez, K.; Avila, C.; Limongi, R.; Vanegas, H.; Vazquez, E. Metamizol, a Non-Opioid Analgesic, Acts via Endocannabinoids in the PAG-RVM Axis during Inflammation in Rats. *Eur. J. Pain* **2012**, *16*, 676–689. [[CrossRef](#)] [[PubMed](#)]
23. Dos Santos, G.G.; Dias, E.V.; Teixeira, J.M.; Athie, M.C.P.; Bonet, I.J.M.; Tambeli, C.H.; Parada, C.A. The Analgesic Effect of Dipyrrone in Peripheral Tissue Involves Two Different Mechanisms: Neuronal KATP Channel Opening and CB1 Receptor Activation. *Eur. J. Pharmacol.* **2014**, *741*, 124–131. [[CrossRef](#)] [[PubMed](#)]
24. Duggan, K.C.; Hermanson, D.J.; Musee, J.; Prusakiewicz, J.J.; Scheib, J.L.; Carter, B.D.; Banerjee, S.; Oates, J.A.; Marnett, L.J. (R)-Profens Are Substrate-Selective Inhibitors of Endocannabinoid Oxygenation by COX-2. *Nat. Chem. Biol.* **2011**, *7*, 803–809. [[CrossRef](#)] [[PubMed](#)]
25. Karlsson, J.; Fowler, C.J. Inhibition of Endocannabinoid Metabolism by the Metabolites of Ibuprofen and Flurbiprofen. *PLoS ONE* **2014**, *9*, e103589. [[CrossRef](#)]
26. Malkowski, M.G.; Ginell, S.L.; Smith, W.L.; Garavito, R.M. The Productive Conformation of Arachidonic Acid Bound to Prostaglandin Synthase. *Science* **2000**, *289*, 1933–1937. [[CrossRef](#)] [[PubMed](#)]
27. Montalbetti, C.A.G.N.; Falque, V. Amide Bond Formation and Peptide Coupling. *Tetrahedron* **2005**, *61*, 10827–10852. [[CrossRef](#)]
28. Fones, W.S. The Use of Sodium Hydride in the Alkylation of N-Substituted Amides. *J. Org. Chem.* **1949**, *14*, 1099–1102. [[CrossRef](#)]
29. Bordwell, F.G.; Fried, H.E. Acidities of the Hydrogen-Carbon Protons in Carboxylic Esters, Amides, and Nitriles. *J. Org. Chem.* **1981**, *46*, 4327–4331. [[CrossRef](#)]
30. Bordwell, F.G.; Ji, G.Z. Effects of Structural Changes on Acidities and Homolytic Bond Dissociation Energies of the Hydrogen-Nitrogen Bonds in Amidines, Carboxamides, and Thiocarboxamides. *J. Am. Chem. Soc.* **1991**, *113*, 8398–8401. [[CrossRef](#)]
31. Schneider, P.; Hosseiny, S.S.; Szczotka, M.; Jordan, V.; Schlitter, K. Rapid Solubility Determination of the Triterpenes Oleanolic Acid and Ursolic Acid by UV-Spectroscopy in Different Solvents. *Phytochem. Lett.* **2009**, *2*, 85–87. [[CrossRef](#)]
32. Cisneros, J.A.; Robertson, M.J.; Mercado, B.Q.; Jorgensen, W.L. Systematic Study of Effects of Structural Modifications on the Aqueous Solubility of Drug-like Molecules. *ACS Med. Chem. Lett.* **2017**, *8*, 124–127. [[CrossRef](#)]
33. Fujita, T.; Iwasa, J.; Hansch, C. A New Substituent Constant, π , Derived from Partition Coefficients. *J. Am. Chem. Soc.* **1964**, *86*, 5175–5180. [[CrossRef](#)]
34. Di, L.; Kerns, E.; Carter, G. Drug-Like Property Concepts in Pharmaceutical Design. *Curr. Pharm. Des.* **2009**, *15*, 2184–2194. [[CrossRef](#)] [[PubMed](#)]
35. Fortuna, A.; Alves, G.; Soares-Da-Silva, P.; Falcão, A. Optimization of a Parallel Artificial Membrane Permeability Assay for the Fast and Simultaneous Prediction of Human Intestinal Absorption and Plasma Protein Binding of Drug Candidates: Application to Dibenz[b,f]Azepine-5-Carboxamide Derivatives. *J. Pharm. Sci.* **2012**, *101*, 530–540. [[CrossRef](#)] [[PubMed](#)]
36. Navarro, G.; Morales, P.; Rodríguez-Cueto, C.; Fernández-Ruiz, J.; Jagerovic, N.; Franco, R. Targeting Cannabinoid CB2 Receptors in the Central Nervous System. Medicinal Chemistry Approaches with Focus on Neurodegenerative Disorders. *Front. Neurosci.* **2016**, *10*, 406. [[CrossRef](#)] [[PubMed](#)]
37. Zhu, C.; Jiang, L.; Chen, T.-M.; Hwang, K.-K. A Comparative Study of Artificial Membrane Permeability Assay for High Throughput Profiling of Drug Absorption Potential. *Eur. J. Med. Chem.* **2002**, *37*, 399–407. [[CrossRef](#)] [[PubMed](#)]
38. Pérez, D.I.; Pistolozzi, M.; Palomo, V.; Redondo, M.; Fortugno, C.; Gil, C.; Felix, G.; Martinez, A.; Bertucci, C. 5-Imino-1,2,4-Thiadiazoles and Quinazolines Derivatives as Glycogen Synthase Kinase 3 β (GSK-3 β) and Phosphodiesterase 7 (PDE7) Inhibitors: Determination of Blood–Brain Barrier Penetration and Binding to Human Serum Albumin. *Eur. J. Pharm. Sci.* **2012**, *45*, 677–684. [[CrossRef](#)] [[PubMed](#)]

39. Konsoula, R.; Jung, M. *In Vitro* Plasma Stability, Permeability and Solubility of Mercaptoacetamide Histone Deacetylase Inhibitors. *Int. J. Pharm.* **2008**, *361*, 19–25. [[CrossRef](#)] [[PubMed](#)]
40. Rodrigues, D.A.; Ferreira-Silva, G.Á.; Ferreira, A.C.S.; Fernandes, R.A.; Kwee, J.K.; Sant'Anna, C.M.R.; Ionta, M.; Fraga, C.A.M. Design, Synthesis, and Pharmacological Evaluation of Novel N -Acylhydrazone Derivatives as Potent Histone Deacetylase 6/8 Dual Inhibitors. *J. Med. Chem.* **2016**, *59*, 655–670. [[CrossRef](#)]
41. Hermans, E. Biochemical and Pharmacological Control of the Multiplicity of Coupling at G-Protein-Coupled Receptors. *Pharmacol. Ther.* **2003**, *99*, 25–44. [[CrossRef](#)] [[PubMed](#)]
42. Howlett, A.C. Cannabinoid Receptor Signaling. In *Cannabinoids*; Springer: Berlin/Heidelberg, Germany, 2005; pp. 53–79.
43. Seamon, K.B.; Padgett, W.; Daly, J.W. Forskolin: Unique Diterpene Activator of Adenylate Cyclase in Membranes and in Intact Cells. *Proc. Natl. Acad. Sci. USA* **1981**, *78*, 3363–3367. [[CrossRef](#)] [[PubMed](#)]
44. Felder, C.C.; Joyce, K.E.; Briley, E.M.; Mansouri, J.; Mackie, K.; Blond, O.; Lai, Y.; Ma, A.L.; Mitchell, R.L. Comparison of the Pharmacology and Signal Transduction of the Human Cannabinoid CB1 and CB2 Receptors. *Mol. Pharmacol.* **1995**, *48*, 443–450. [[PubMed](#)]
45. Khanolkar, A.D.; Palmer, S.L.; Makriyannis, A. Molecular Probes for the Cannabinoid Receptors. *Chem. Phys. Lipids* **2000**, *108*, 37–52. [[CrossRef](#)] [[PubMed](#)]
46. Munro, S.; Thomas, K.L.; Abu-Shaar, M. Molecular Characterization of a Peripheral Receptor for Cannabinoids. *Nature* **1993**, *365*, 61–65. [[CrossRef](#)]
47. Iwamura, H.; Suzuki, H.; Ueda, Y.; Kaya, T.; Inaba, T. *In Vitro* and *in Vivo* Pharmacological Characterization of JTE-907, a Novel Selective Ligand for Cannabinoid CB2 Receptor. *J. Pharmacol. Exp. Ther.* **2001**, *296*, 420–425.
48. Gentili, M.; Ronchetti, S.; Ricci, E.; Di Paola, R.; Gugliandolo, E.; Cuzzocrea, S.; Bereshchenko, O.; Migliorati, G.; Riccardi, C. Selective CB2 Inverse Agonist JTE907 Drives T Cell Differentiation towards a Treg Cell Phenotype and Ameliorates Inflammation in a Mouse Model of Inflammatory Bowel Disease. *Pharmacol. Res.* **2019**, *141*, 21–31. [[CrossRef](#)]
49. Presley, C.; Abidi, A.; Suryawanshi, S.; Mustafa, S.; Meibohm, B.; Moore, B.M. Preclinical Evaluation of SMM-189, a Cannabinoid Receptor 2-specific Inverse Agonist. *Pharmacol. Res. Perspect.* **2015**, *3*, e00159. [[CrossRef](#)]
50. Lunn, C.A.; Reich, E.-P.; Fine, J.S.; Lavey, B.; Kozlowski, J.A.; Hipkin, R.W.; Lundell, D.J.; Bober, L. Biology and Therapeutic Potential of Cannabinoid CB 2 Receptor Inverse Agonists. *Br. J. Pharmacol.* **2008**, *153*, 226–239. [[CrossRef](#)]
51. Cascio, M.G.; Bolognini, D.; Pertwee, R.G.; Palazzo, E.; Corelli, F.; Pasquini, S.; Di Marzo, V.; Maione, S. *In Vitro* and *in Vivo* Pharmacological Characterization of Two Novel Selective Cannabinoid CB2 Receptor Inverse Agonists. *Pharmacol. Res.* **2010**, *61*, 349–354. [[CrossRef](#)]
52. Dubuisson, D.; Dennis, S.G. The Formalin Test: A Quantitative Study of the Analgesic Effects of Morphine, Meperidine, and Brain Stem Stimulation in Rats and Cats. *Pain* **1977**, *4*, 161–174. [[CrossRef](#)] [[PubMed](#)]
53. Hunskaar, S.; Hole, K. The Formalin Test in Mice: Dissociation between Inflammatory and Non-Inflammatory Pain. *Pain* **1987**, *30*, 103–114. [[CrossRef](#)] [[PubMed](#)]
54. Chen, X.; Murawski, A.; Patel, K.; Crespi, C.L.; Balimane, P.V. A Novel Design of Artificial Membrane for Improving the PAMPA Model. *Pharm. Res.* **2008**, *25*, 1511–1520. [[CrossRef](#)] [[PubMed](#)]
55. Lopes, J.P.B.; Silva, L.; Ceschi, M.A.; Lüdtke, D.S.; Zimmer, A.R.; Ruaro, T.C.; Dantas, R.F.; de Salles, C.M.C.; Silva-Jr, F.P.; Senger, M.R.; et al. Synthesis of New Lophine-Carbohydrate Hybrids as Cholinesterase Inhibitors: Cytotoxicity Evaluation and Molecular Modeling. *Medchemcomm* **2019**, *10*, 2089–2101. [[CrossRef](#)] [[PubMed](#)]
56. Xiang, W.; Shi, R.; Kang, X.; Zhang, X.; Chen, P.; Zhang, L.; Hou, A.; Wang, R.; Zhao, Y.; Zhao, K.; et al. Monoacylglycerol Lipase Regulates Cannabinoid Receptor 2-Dependent Macrophage Activation and Cancer Progression. *Nat. Commun.* **2018**, *9*, 2574. [[CrossRef](#)] [[PubMed](#)]
57. Di, L.; Kerns, E.H.; Fan, K.; McConnell, O.J.; Carter, G.T. High Throughput Artificial Membrane Permeability Assay for Blood–Brain Barrier. *Eur. J. Med. Chem.* **2003**, *38*, 223–232. [[CrossRef](#)]
58. Gomes, N.M.; Rezende, C.M.; Fontes, S.P.; Matheus, M.E.; Fernandes, P.D. Antinociceptive Activity of Amazonian Copaiba Oils. *J. Ethnopharmacol.* **2007**, *109*, 486–492. [[CrossRef](#)]